Received: 17 March 2022 | Revised: 31 May 2022 | Accepted: 10 June 2022

DOI: 10.1002/mp.15818

RESEARCH ARTICLE

MEDICAL PHYSICS

Regional left ventricular endocardial strains estimated from low-dose 4DCT: Comparison with cardiac magnetic resonance feature tracking

Ashish Manohar[1] | **Gabrielle M. Colvert**[2] | **Juan E. Ortuño**[3,4] | **Zhennong Chen**[2] | **James Yang**[2] | **Brendan T. Colvert**[2] | **W. Patricia Bandettini**[5] | **Marcus Y. Chen**[5] | **María J. Ledesma-Carbayo**[3,4] | **Elliot R. McVeigh**[2,6,7]

[1]Department of Mechanical and Aerospace Engineering, University of California San Diego, La Jolla, California, USA

[2]Department of Bioengineering, University of California San Diego, La Jolla, California, USA

[3]Biomedical Research Networking Centre in Bioengineering, Biomaterials and Nanomedicine, Madrid, Spain

[4]Biomedical Image Technologies Laboratory, ETSI Telecomunicación, Universidad Politécnica de Madrid, Madrid, Spain

[5]National Heart, Lung, and Blood Institute, National Institutes of Health, Bethesda, Maryland, USA

[6]Department of Radiology, University of California San Diego, La Jolla, California, USA

[7]Department of Medicine, Cardiovascular Division, University of California San Diego, La Jolla, California, USA

Correspondence
Elliot R. McVeigh, 9452 Medical Center Drive, La Jolla, CA 92037, USA.
Email: emcveigh@ucsd.edu

Ashish Manohar and Gabrielle M. Colvert contributed equally, and are cofirst authors

Funding information
National Institutes of Health, Grant/Award Numbers: F31HL151183, T32HL105373, R01HL144678, 1ZIAHL006220; American Heart Association, Grant/Award Number: 20PRE35210261

Abstract

Background: Estimates of regional left ventricular (LV) strains provide additional information to global function parameters such as ejection fraction (EF) and global longitudinal strain (GLS) and are more sensitive in detecting abnormal regional cardiac function. The accurate and reproducible assessment of regional cardiac function has implications in the management of various cardiac diseases such as heart failure, myocardial ischemia, and dyssynchrony.

Purpose: To develop a method that yields highly reproducible, high-resolution estimates of regional endocardial strains from 4DCT images.

Methods: A method for estimating regional LV endocardial circumferential (ϵ_{cc}) and longitudinal (ϵ_{ll}) strains from 4DCT was developed. Point clouds representing the LV endocardial surface were extracted for each time frame of the cardiac cycle from 4DCT images. 3D deformation fields across the cardiac cycle were obtained by registering the end diastolic point cloud to each subsequent point cloud in time across the cardiac cycle using a 3D point-set registration technique. From these deformation fields, ϵ_{cc} and ϵ_{ll} were estimated over the entire LV endocardial surface by fitting an affine transformation with maximum likelihood estimation. The 4DCT-derived strains were compared with strains estimated in the same subjects by cardiac magnetic resonance (CMR); twenty-four subjects had CMR scans followed by 4DCT scans acquired within a few hours. Regional LV circumferential and longitudinal strains were estimated from the CMR images using a commercially available feature tracking software (cvi42). Global circumferential strain (GCS) and global longitudinal strain (GLS) were calculated as the mean of the regional strains across the entire LV for both modalities. Pearson correlation coefficients and Bland-Altman analyses were used for comparisons. Intraclass correlation coefficients (ICC) were used to assess the inter- and intraobserver reproducibility of the 4DCT-derived strains.

Results: The 4DCT-derived regional strains correlated well with the CMR-derived regional strains (ϵ_{cc}: $r = 0.76$, $p < 0.001$; ϵ_{ll}: $r = 0.64$, $p < 0.001$). A very strong correlation was found between 4DCT-derived GCS and 4DCT-derived EF ($r = -0.96$; $p < 0.001$). The 4DCT-derived strains were also highly reproducible, with very low inter- and intraobserver variability (intraclass correlation coefficients in the range of [0.92, 0.99]).

Conclusions: We have developed a novel method to estimate high-resolution regional LV endocardial circumferential and longitudinal strains from 4DCT images. Except for the definition of the mitral valve and LV outflow tract planes,

 © 2022 American Association of Physicists in Medicine.

the method is completely user independent, thus yielding highly reproducible estimates of endocardial strain. The 4DCT-derived strains correlated well with those estimated using a commercial CMR feature tracking software. The promising results reported in this study highlight the potential utility of 4DCT in the precise assessment of regional cardiac function for the management of cardiac disease.

KEYWORDS
4DCT, cardiac CT, LV function, LV myocardial strain

1 | INTRODUCTION

The accurate and reproducible assessment of regional cardiac function has implications in the management of various cardiac diseases such as heart failure,[1] myocardial ischemia,[2] and dyssynchrony.[3] Regional left ventricular (LV) strains provide essential information in addition to ejection fraction (EF); they are more sensitive measures for detecting abnormal cardiac function and they can be earlier predictors of mortality and cardiac events.[4–6]

Modern four-dimensional X-ray computed tomography (4DCT) imaging systems can acquire full three-dimensional (3D) images spanning the entire superior-inferior extent of the heart across the entire cardiac cycle from a single table position and within a single heartbeat. Additionally, the images are now acquired with low patient exposure to ionizing radiation[7,8]; new high-resolution detectors and photon-counting computed tomography (CT) will lead to further improvements.[9] The images have high spatial resolution,[10] delineating the fine endocardial texture of the LV comprising the papillary muscles and trabeculae carneae[11]; these features can serve as fiducial markers for 3D motion tracking.[12,13] The temporal resolution of 4DCT is ~65 ms for dual-source scanners and ~140 ms for single-source scanners; however, with effective motion correction technologies, the temporal resolution of single-source scanners can be significantly improved.[14]

While transthoracic echocardiography is the most widely used cardiac imaging modality with excellent temporal resolution and established disease diagnosis guidelines,[15] the recent advances in 4DCT imaging have made it a promising tool to assess regional cardiac function, especially as a low dose adjunct to excellent coronary CT angiography (CCTA). CCTA is rapidly becoming an important diagnostic method for patient management and for assessing future risk of cardiovascular events.[16] 4DCT of cardiac function can be simultaneously obtained in the same heartbeat as the CCTA exam. Superb functional information from all chambers is then available, and this would also eliminate the need to separately image the patient with either CMR or echocardiography for functional analysis. This is the primary motivation to develop functional analysis from 4DCT data.

Previous studies have used 4DCT to estimate LV myocardial function.[17–21] Lamash et al. used a deformable LV model to estimate regional and global myocardial strains from 3D velocity fields which were extracted via a novel optical flow technique.[17] The model was then used to successfully differentiate between normal and abnormal myocardial segments in a cohort of 93 subjects with cardiac 4DCT scans.[20] Vach et al. used 4DCT to estimate regional myocardial strain in a cohort of 43 subjects with advanced cardiac valve disease.[21] A commercially available CT strain software was used to derive highly reproducible estimates of regional myocardial strain from the 4DCT images, which were then compared with strain estimates derived from transthoracic echocardiography. These studies have convincingly demonstrated the potential utility of 4DCT for the routine clinical evaluation of regional myocardial function; however, they estimate myocardial strain by employing the use of smooth endocardial and epicardial contours, which can lead to erroneous estimates. Therefore, we sought to develop a method to estimate regional endocardial strains that is free from contouring by leveraging the region of the cardiac 4DCT images with maximum contrast: the boundary between the myocardium and the LV blood pool.

We have previously estimated endocardial regional shortening (RS_{CT}) from 4DCT images,[12,22] which is similar to local strain, but it does not distinguish between circumferential and longitudinal strains. RS_{CT} is very reproducible and has been validated using in silico phantom experiments[13] and cardiac magnetic resonance (CMR) tagging in canine hearts.[23] Additionally, RS_{CT} maps have been used to characterize the regionally heterogenous effects of mitral regurgitation and transcatheter mitral valve implantation (TMVI) on LV function.[24] RS_{CT} is very stable and robust, as it estimates shortening independent of the cardiac coordinate system.

In this work, we develop a novel technique that measures two *directional* endocardial cardiac strains: circumferential strain ϵ_{cc}^{CT} and longitudinal strain ϵ_{ll}^{CT}. These strains have prognostic value in patients with specific cardiac diseases.[25] Additionally, we compare the

4DCT-derived regional endocardial strains with those estimated using a commercial CMR feature tracking software (cvi42) in 24 subjects who had both 4DCT and CMR scans acquired a few hours apart.

2 | METHODS

2.1 | Subjects

Twenty-four consecutive subjects with full cardiac cycle and full LV volume retrospective ECG-gated CT angiography (CTA) and CMR exams were used in this study. All subjects were scanned under IRB approved protocols at the U.S. National Institutes of Health (NIH), Bethesda, Maryland. These subjects were enrolled in a study to evaluate coronary artery disease (CAD) characterized by CTA and to evaluate valve and aortic disease using CMR.

2.2 | Image acquisition

2.2.1 | 4DCT

Single-heartbeat, tube current modulated, retrospective ECG-gated CTA images were acquired from a single table position during an inspiratory breath-hold on a 320 detector-row scanner (Aquilion ONE, Canon Medical Systems, Otawara, Japan). The gantry rotation time was 275 ms. LV blood pool contrast enhancement was achieved by injecting a nonionic radiocontrast agent (Isovue 370, Bracco Diagnostics, Princeton, NJ) at the rate of 5 ml/s via a triphasic protocol comprising 49 ml of contrast agent followed by a 20 ml mixture of 30% contrast agent and 70% saline, followed by 50 mL of saline. Bolus tracking (SureStart, Canon Medical Systems, Otawara, Japan) was started in the descending aorta 16 s after contrast injection and entire heart volume imaging was triggered within 1 second of reaching a threshold of 400 HU in the descending aorta. Each acquisition was dose modulated with the X-ray tube current at maximum only during diastasis and at 20% of the maximum at all other time points through the single R–R interval, resulting in a dose reduction of 50–75% compared with full retrospective scanning. The diastasis tube currents applied were in the range of [210, 820] mA (n = 19; median: 420 mA; interquartile range: 173 mA) at 100 kVp and 750 mA at 120 kVp (n = 6). Images were reconstructed using the Cardiac FC03 kernel into 512 × 512 × 320 grids, with in-plane pixel spacings of 0.4 mm in the x–y directions and slice thicknesses of 0.5 mm in z. The mean contrast-to-noise ratio (CNR) between the LV blood pool and the myocardium was 10.1 ± 3.1. Figure 1 shows multiplanar reconstruction (MPR) views of a 4DCT acquisition in one of the subjects.

2.2.2 | CMR

Cine CMR images were acquired using a 1.5T scanner (MAGNETOM Aera, Siemens Healthineers, Erlangen, Germany). Three long-axis planes (2-chamber, 4-chamber, and parasternal) and nine evenly spaced short-axis planes from base to apex were acquired with an ECG-triggered, fast imaging with steady-state precession (TrueFISP, Siemens Healthineers, Erlangen, Germany) protocol. The slice thicknesses were in the range of [6, 8] mm. Figure 2 shows the CMR-acquired planes for the same subject shown in Figure 1.

2.3 | Regional strain estimation

2.3.1 | 4DCT-derived regional *endocardial* strain

Each time frame of the LV blood pool in a 4DCT dataset was segmented using the active contour region growing module of ITK-SNAP v3.6.2.[26] The highly automated segmentation procedure has been previously described in detail.[24] A point cloud defining the endocardial surface was extracted from each segmented LV blood pool volume. A nonrigid point-set registration technique[27] was used to register the end diastolic point cloud (*template* point cloud) to subsequent point clouds (*target* point clouds) segmented from other time frames of the cardiac cycle. The registration algorithm estimates a smooth 3D displacement field mapping the template point cloud to each target point cloud; using these estimated displacement fields, the points in the template point cloud are then warped into specific poses to create the best representations of the target point clouds. Since there is a 1:1 correspondence between the template point cloud and the deformed point clouds representing the targets, regional strains can be directly computed. This is equivalent to "point tracking" of a set of endocardial material points. Figure 3a summarizes the procedure outlined above. This method of obtaining 3D endocardial displacement fields has been described in detail previously.[13,22,24]

Figure 3b shows the new method of deriving endocardial strains from the 3D displacement fields. Fifteen percent of the total number of points in the end diastolic point cloud were randomly selected to serve as centers of endocardial patches p of radii 7.5 mm each to uniformly sample the entire endocardial surface. This 7.5-mm radius matched the optimal spatial resolution of the 3D point set registration technique for detecting regional wall motion abnormalities with high accuracy.[13] A normal sized human LV has ∼4000 points in its end diastolic point cloud; thus, ∼600 patch centers were selected to sample the entire LV endocardial surface. The displacement of a point within a patch p was then

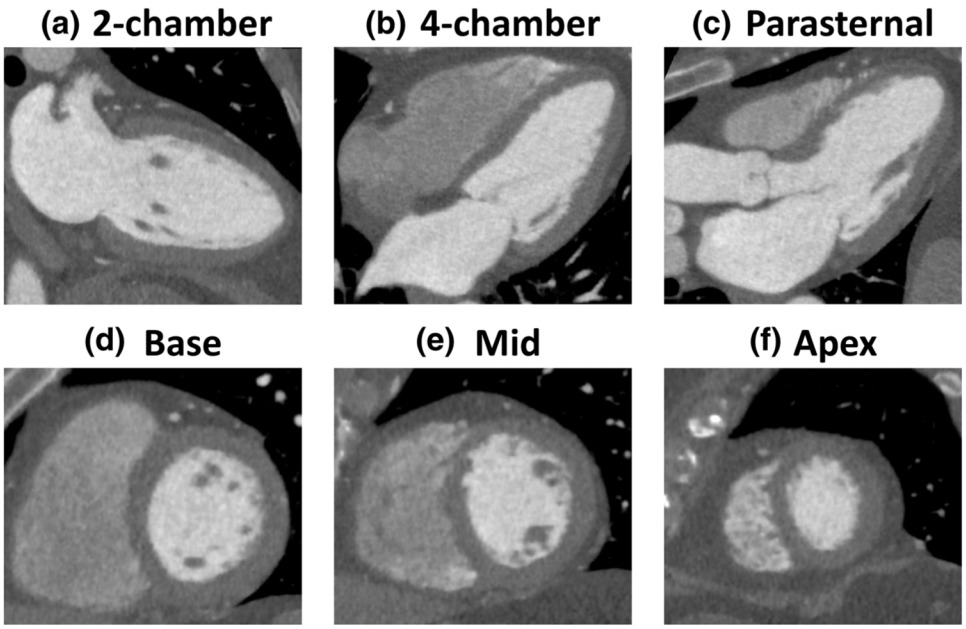


FIGURE 1 MPR views of a 4DCT acquisition. (a) 2-chamber view. (b) 4-chamber view. (c) Parasternal view. (d) Short-axis basal plane. (e) Short-axis mid plane. (f) Short-axis apical plane.
Abbreviation: MPR, multi-planar reconstruction

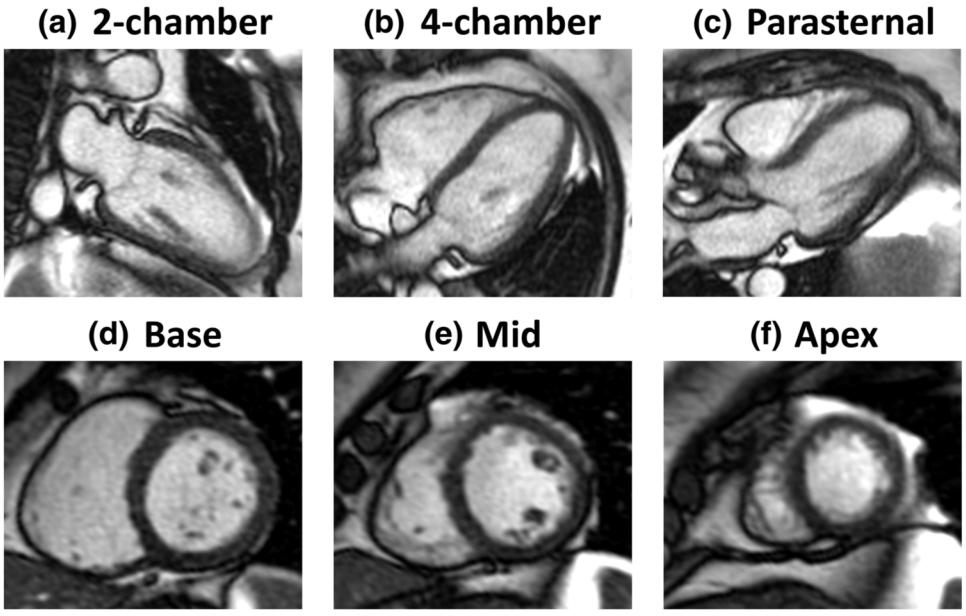


FIGURE 2 Planes acquired during a CMR scan (same subject as Figure 1) (a) 2-chamber view. (b) 4-chamber view. (c) Parasternal view. (d) Short-axis basal plane. (e) Short-axis mid plane. (f) Short-axis apical plane.
Abbreviation: CMR, cardiac magnetic resonance.

modeled as an affine transformation according to the equation:

$$\boldsymbol{y} = \boldsymbol{A}^{(p)}\ \boldsymbol{x} + \boldsymbol{b}^{(p)} + \eta\left(\sigma^{(p)}\right), \tag{1}$$

where $\boldsymbol{A}$ is the 3×3 affine transformation matrix, $\boldsymbol{b}$ is the translation vector, and $\boldsymbol{y}$ is the new displaced position of point $\boldsymbol{x}$ within patch p. A residual term, η, is included in the motion model to account for noise. It was assumed that the residual term is normally

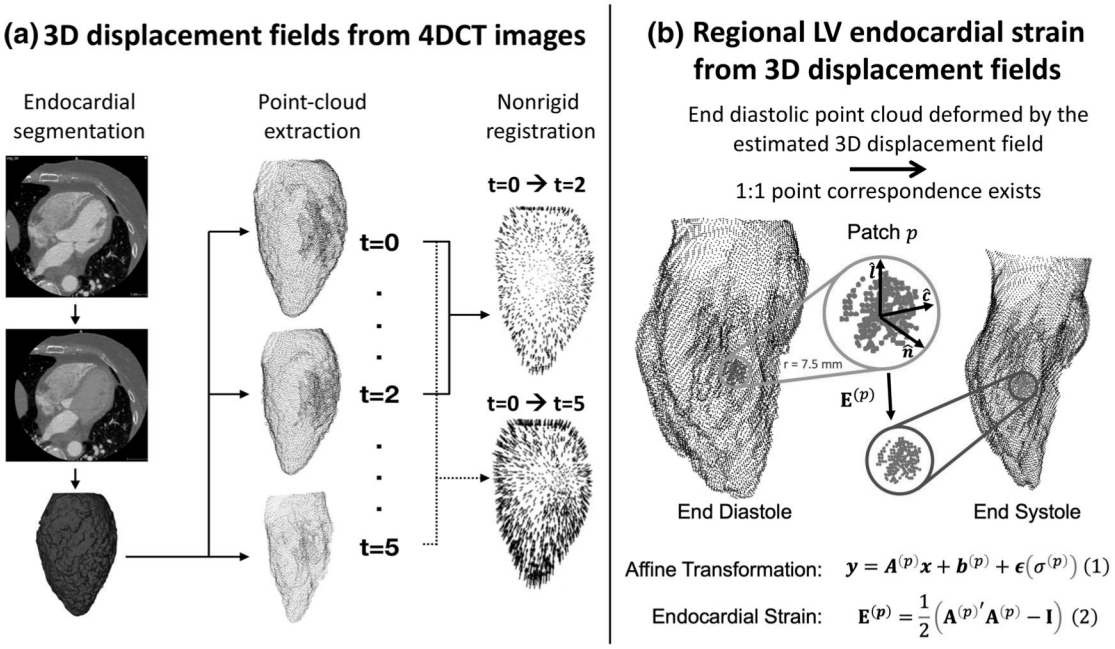


FIGURE 3 Estimation of regional LV endocardial strain from 3D displacement fields derived from 4DCT images. (a) 3D displacement fields are derived from 4DCT images in 3 steps: (1) segmentation of the LV blood pool for all time frames across the cardiac cycle in the 4DCT dataset, (2) extraction of a point-cloud defining the endocardial surface from each segmented LV image, and (3) nonrigid registration of the end diastolic point cloud to subsequent point clouds across the cardiac cycle. (b) Regional endocardial strain is estimated from the displacement fields by sampling the endocardial surface in patches of radius 7.5 mm. The deformation of each patch, p, is modeled as an affine transformation and maximum likelihood estimation is used to fit the motion model. The affine transformation matrix, $\boldsymbol{A}^{(p)}$, is used to calculate the strain tensor, $\boldsymbol{E}^{(p)}$, which is then rotated into cardiac coordinates to obtain longitudinal (ε_{ll}^{CT}) and circumferential (ε_{cc}^{CT}) strains.
Abbreviation: LV, left ventricle.

distributed and governed by the standard deviation σ which is also computed in the algorithm. Maximum likelihood estimation was used to solve for the unknown parameters $\boldsymbol{A}$, $\boldsymbol{b}$, and σ for each patch p. The 3D strain tensor was then estimated according to the following equation:

$$\boldsymbol{E}^{(p)} = \frac{1}{2}\left(\boldsymbol{A}^{(p)'}\boldsymbol{A}^{(p)} - \boldsymbol{I}\right), \quad (2)$$

where $\boldsymbol{E}^{(p)}$ is the Green-Lagrangian strain tensor for a patch p and $\boldsymbol{I}$ is the identity matrix. $\boldsymbol{E}^{(p)}$ was then rotated into the cardiac frame of reference to obtain the longitudinal and circumferential strain components, as shown in Figure 3b. The regional endocardial strains sampled at the ~600 patch locations were linearly interpolated to all other points in the point cloud defining the endocardial surface. In order to compare with CMR derived strains, regional circumferential (ε_{cc}^{CT}) and regional longitudinal (ε_{ll}^{CT}) strains were calculated for the standard AHA 16 segment model of the LV.[28] Global circumferential strain (GCS_{CT}) and global longitudinal strain (GLS_{CT}) of the endocardium were calculated as the average of the end systolic strains across all 16 AHA segments.

2.3.2 | CMR-derived regional *myocardial* strain

Regional LV strain estimates were derived from the CMR images using a commercial feature tracking strain estimation software (cvi42, Circle Cardiovascular Imaging Inc., Calgary, Canada). cvi42 estimates both 2D and 3D strains; for this study, only the 3D strains were recorded to facilitate a direct comparison with the 4DCT-derived regional endocardial strains. The first image after the ECG trigger of the CMR series was set as end diastole; end systole was set as the phase with minimum LV volume. The endocardial and epicardial contours were automatically detected by the software. For the 3D strain analysis, the detected endo- and epicardial contours were interpolated in both the short- and long-axis views to create a deformable 3D model of the myocardium. The 3D strain estimation procedure using cvi42 has been described in detail previously.[29,30] Figure 4a shows the mesh representations of the output of the feature tracking method overlaid onto the short-axis mid plane, the 2-chamber, the 4-chamber, and the parasternal views for the end diastolic and end systolic frames in a subject.

The estimates of regional strain from cvi42 were computed as the average strain in each myocardial segment

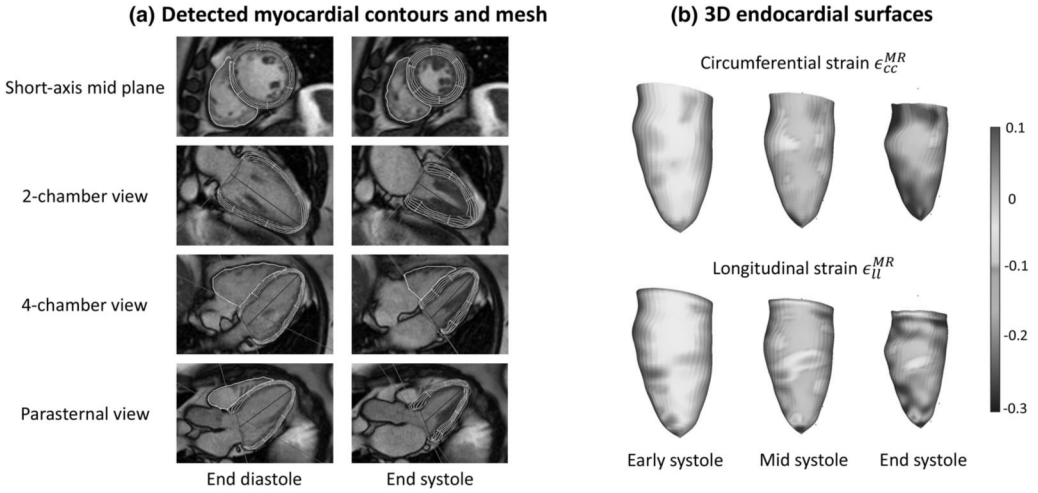


FIGURE 4 Estimation of LV myocardial strain with cvi42. (a) Automated detection of endocardial and epicardial contours defining a mesh model of the LV myocardium at both end diastole (left column) and end systole (right column) for four different imaging planes. (b) Regional myocardial strains mapped onto smooth 3D renderings of the endocardial surfaces at three time points of the cardiac cycle. *Abbreviations*: ϵ_{cc}^{MR}, CMR-derived regional circumferential strain; ϵ_{ll}^{MR}, CMR-derived regional longitudinal strain; LV, left ventricle.

of the standard AHA 16 segment model of the LV,[28] not the endocardial strain. Both regional circumferential (ϵ_{cc}^{MR}) and regional longitudinal (ϵ_{ll}^{MR}) strains were recorded. Global circumferential (GCS_{MR}) and global longitudinal (GLS_{MR}) strains were calculated as the mean of the end systolic regional strain values across all 16 AHA segments. Figure 4b shows the circumferential and longitudinal strain values estimated using cvi42 at early systole, mid systole, and end systole mapped onto a smooth representation of the endocardial surface.

2.4 | Statistical analysis

Bland-Altman and correlation plots were used to describe the relationship between the 4DCT- and the CMR-derived regional strains. Regional strains at three time points during systole (early, mid, and end systole) were compared, ensuring that a broad dynamic range of strain values were included. Additionally, *GCS* and *GLS* derived from both the 4DCT and the CMR images were plotted against the corresponding left ventricular ejection fractions (LVEFs) for each modality. Lastly, the relationship between the 4DCT- and CMR-derived end diastolic (EDV) and end systolic (ESV) volumes was also investigated. Linear models were used to describe each of the above relationships, and a p-value < 0.05 was considered significant for the correlation coefficient.

2.5 | Reproducibility analysis

The reproducibility of the proposed 4DCT-derived strain estimation method was investigated using two observers; both observers (1 and 2) were PhD Candidates in engineering, and each had 7 years of experience in analyzing cardiac images. Ten subjects were randomly selected from the cohort of 24 subjects used in the study. For each of the 10 subjects, the LV blood pool was segmented from the end diastolic and the end systolic time frames (as described in Sec. 2.3.1) by both observers independently. To investigate the intraobserver reproducibility, observer 1 performed the segmentations for a second time; the two rounds of segmentations were separated by 10 days. Intraclass correlation coefficients (ICC) were then calculated for both end systolic regional (ϵ_{cc}^{CT} and ϵ_{ll}^{CT}) and end systolic global (GCS_{CT} and GLS_{CT}) strain estimates for all 10 subjects using a two-way absolute agreement model. Based on the ICC, the reproducibility was categorized as either poor (ICC $\leq$ 0.5), good (0.5 $<$ ICC $\leq$ 0.75), or excellent (ICC $>$ 0.75). Additionally, the range of EDV and ESV between the three rounds of segmentations (two by observer 1 and one by observer 2) was determined for all 10 subjects.

3 | RESULTS

3.1 | Subjects

Of the 24 subjects used in the study, eight were female (33%). The average age of the subjects was 55 $\pm$ 14 years. The mean CT-derived EF was 69 $\pm$ 8%, and no subject was diagnosed with either heart failure, myocardial infarction, nor atrial fibrillation. One subject was diagnosed with obstructive coronary artery disease. The mean CT dose index-volume (CTDIvol) was 16.6 $\pm$ 11.5

TABLE 1 Subject characteristics

N	24
Age (years)	55 ± 14
Female (%)	8 (33)
Body mass index (kg/m^2), [max. value]	27.9 ± 4.3 [35.3]
4DCT-derived EF (%)	69 ± 8
Time between CMR and CT scans (h)	4.1 ± 1.5
Obstructive coronary artery disease (%)	1 (4)
Atrial fibrillation (%)	0 (0)
Mild/moderate aortic stenosis (%)	5 (21)
Bioprosthetic aortic valve (%)	3 (13)
Myocardial infarction (%)	0 (0)
Diabetes mellitus (%)	1 (4)
Congestive heart failure (%)	0 (0)
Smoker (%)	7 (29)
Hyperlipidemia (%)	15 (63)
Hypertension (%)	11 (46)
CTDIvol (mGy)	16.6 ± 11.5
DLP (mGy × cm)	198.4 ± 134.6

Abbreviations: CMR, cardiac magnetic resonance; CT, computed tomography; CTDIvol, CT dose index-volume; DLP, dose length product; EF, ejection fraction.

mGy, and the mean dose length product (DLP) was 198.4 mGy × cm ± 134.6 mGy × cm. Table 1 lists the subject characteristics.

3.2 | 4DCT- and CMR-derived regional strains

The proposed 4DCT analysis method yields high-resolution estimates of regional endocardial strains. Figure 5 shows 3D renderings of the LV endocardial surface for a subject at six phases of the cardiac cycle with 4DCT-derived regional circumferential (ε_{cc}^{CT}; Figure 5a) and regional longitudinal (ε_{ll}^{CT}; Figure 5b) strains mapped onto the endocardium. Blue represents contraction and yellow represents stretch.

Figure 6 shows the relationship between the 4DCT-derived and the CMR-derived regional strains. Figures 6a,b show the relationship between ϵ_{cc}^{CT} and ϵ_{cc}^{MR} and Figures 6c,d show the relationship between ϵ_{ll}^{CT} and ϵ_{ll}^{MR}. The regional circumferential strains were strongly correlated with a correlation coefficient of 0.76 ($p < 0.001$), while the regional longitudinal strains were moderately correlated with a correlation coefficient of 0.64 ($p < 0.001$). The slopes of the linear fits between the 4DCT- and the CMR-derived regional strains were 0.56 and 0.49 for ϵ_{cc} and ϵ_{ll}, respectively. The Bland-Altman analysis revealed that the ϵ_{cc}^{CT} estimates were biased with higher magnitude by 6.3%, while the ϵ_{ll}^{CT} estimates were biased with higher magnitude by 2.8%.

Additionally, Figure 7 shows the relationship between *GCS* and EF, and *GLS* and EF for each modality. Figures 7a,b show the relationship between GCS_{CT} and GLS_{CT} with 4DCT-derived EF (EF_{CT}), while Figures 7c,d show the relationship between GCS_{MR} and GLS_{MR} with CMR-derived EF (EF_{MR}). All global strains were moderately correlated with EF, except for GCS_{CT} which was very strongly correlated with EF_{CT} ($r = -0.96$; $p < 0.001$).

Figure 8 shows the relationship between the 4DCT- and CMR-derived EDV and ESV estimates for all 24 subjects used in the study. The volumes derived from the two modalities were strongly correlated, with a Pearson correlation coefficient of 0.97. The CMR volumes were derived from myocardial contours, while the CT volumes were computed by simply counting the voxels of the segmented LV blood volume. Larger dilated hearts had more blood volume above the LV outflow tract—this volume was cut off with standard contouring tools used in CMR. Also, smooth CMR contours drawn on the end systolic frames included significant trabecular tissue and papillary muscles within the LV volume, leading to larger ESVs for CMR.

3.3 | Reproducibility analysis

Results from the inter- and intraobserver reproducibility analysis are provided in Table 2. All 4DCT-derived regional and global strain estimates were highly reproducible, with ICCs in the range of [0.92, 0.99] for interobserver variability and [0.96, 0.99] for intraobserver variability. The range of differences in EDV and ESV between the three independent rounds of segmentations over all 10 subjects was 2.2 ± 1.7 ml (max. difference: 5.5 ml) and 1.4 ± 0.7 ml (max. difference: 2.7 ml), respectively. The mean EDV and ESV for the 10 subjects were 114 ± 27 ml and 37 ± 16 ml; thus, the range in estimated LV volumes between the three rounds of segmentations represents a 2% and a 4% variability in EDV and ESV, respectively.

4 | DISCUSSION

The paper describes a method to compute highly reproducible, high-resolution endocardial strain estimates from clinical 4DCT images. The method was tested on a cohort of 24 consecutive subjects that underwent both 4DCT and CMR exams within a few hours of each other. The 4DCT-derived regional endocardial strains correlated well with those derived using a commercial CMR feature tracking strain estimation software. The main findings reveal the potential utility of 4DCT in obtaining highly reproducible, high-resolution endocardial strain estimates that may be obtained simultaneously from the same acquisition as coronary CTA (CCTA) with small

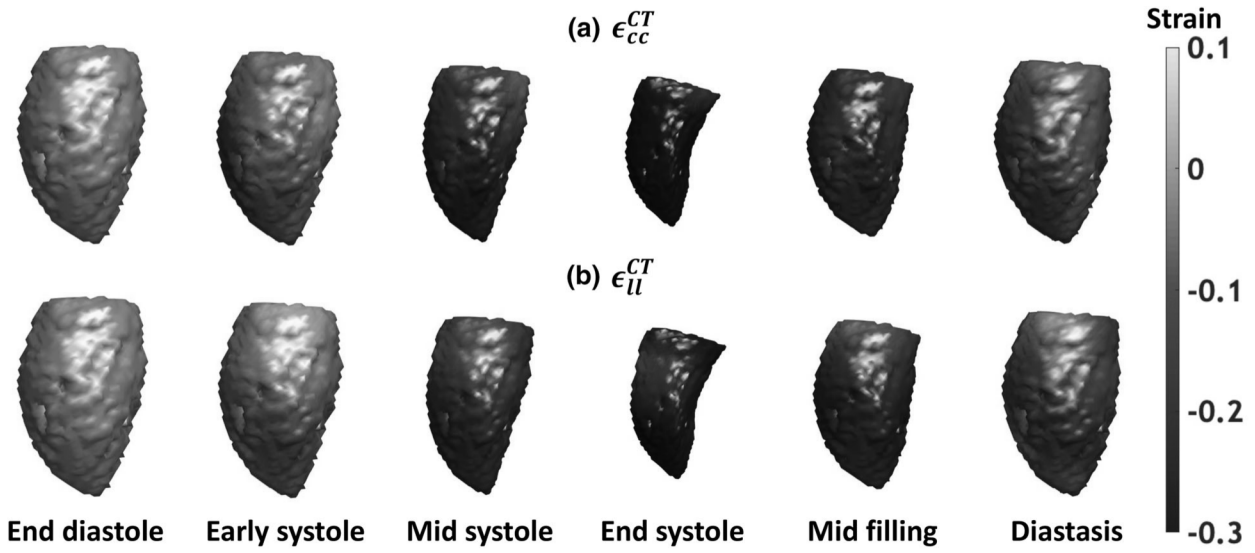


FIGURE 5 High-resolution maps of 4DCT-derived regional endocardial strains in an example subject. (a) ϵ_{cc}^{CT} values mapped onto the endocardial surface. (b) ϵ_{ll}^{CT} values mapped onto the endocardial surface. All views are of the 3D endocardial lateral wall, with the anterior wall to the left and the inferior wall to the right. Blue represents contraction and yellow represents stretch.
Abbreviations: ϵ_{cc}^{CT}, 4DCT-derived regional circumferential strain; ϵ_{ll}^{CT}, 4DCT-derived regional longitudinal strain.

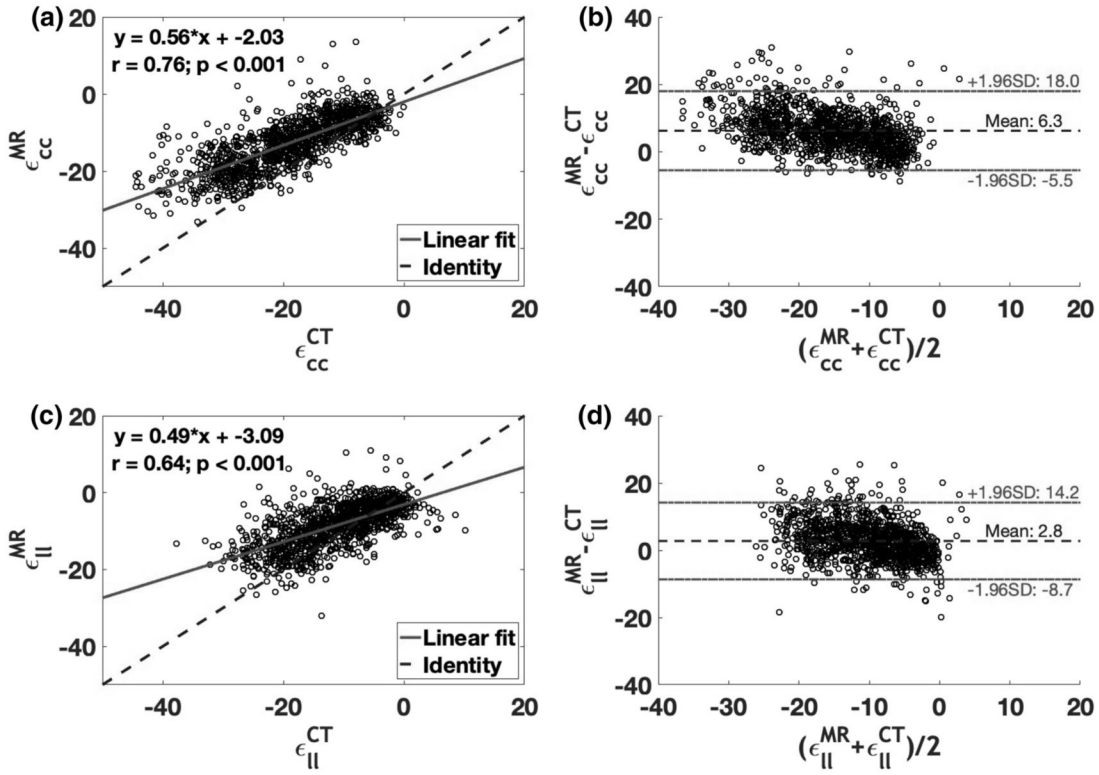


FIGURE 6 Relationship between 4DCT- and CMR-derived regional LV strains. (a–b) Relationship between ϵ_{cc}^{CT} and ϵ_{cc}^{MR} using (a) direct comparison and (b) Bland-Altman analysis. (c–d) Relationship between ϵ_{ll}^{CT} and ϵ_{ll}^{MR} using (c) direct comparison and (d) Bland-Altman analysis.
Abbreviations: ϵ_{cc}^{CT}, 4DCT-derived regional circumferential strain; ϵ_{cc}^{MR}, CMR-derived regional circumferential strain; ϵ_{ll}^{CT}, 4DCT-derived regional longitudinal strain; ϵ_{ll}^{MR}, CMR-derived regional longitudinal strain.

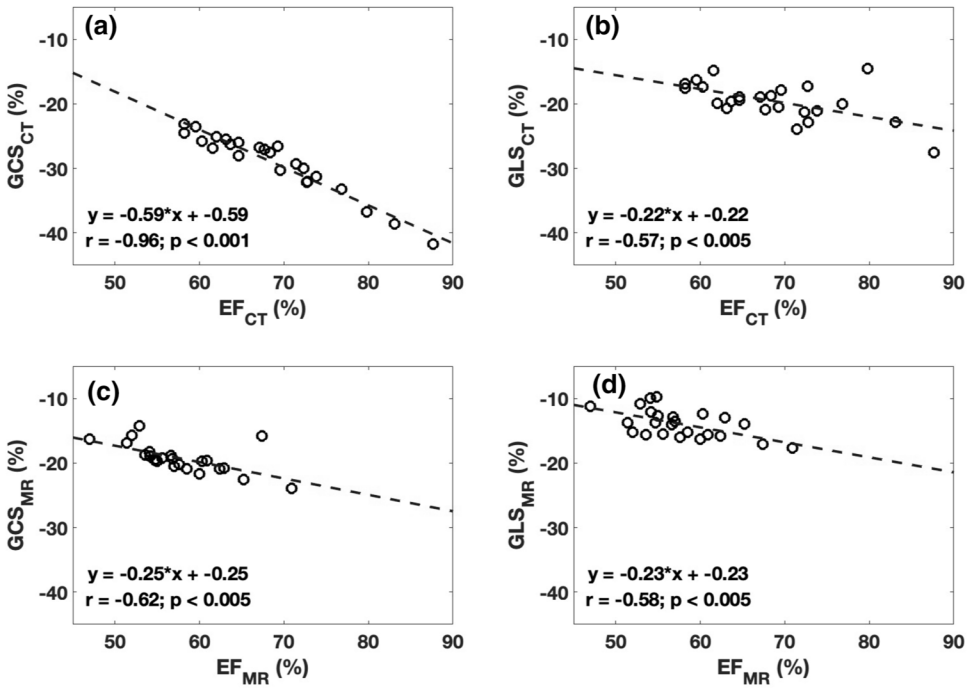


FIGURE 7 Relationship between 4DCT- and CMR-derived GCS and GLS with EF. (a–b) Relationship between EF_{CT} and (a) GCS_{CT} and (b) GLS_{CT}. (c–d) Relationship between EF_{MR} and (c) GCS_{MR} and (d) GLS_{MR}.
Abbreviations: EF_{CT}, 4DCT – derived ejection fraction; EF_{MR}, CMR – derived ejection fraction; GCS_{CT}, 4DCT-derived global circumferential strain; GLS_{CT}, 4DCT-derived global longitudinal strain; GCS_{MR}, CMR-derived global circumferential strain; GLS_{MR}, CMR-derived global longitudinal strain.

TABLE 2 Inter- and intraobserver reproducibility for end systolic regional and global strains

Strain estimate	Interobserver reproducibilityICC (95% CI)	Intraobserver reproducibilityICC (95% CI)
ϵ_{cc}^{CT}	0.95 (0.93–0.96)	0.99 (0.98–0.99)
ϵ_{ll}^{CT}	0.92 (0.89–0.94)	0.96 (0.95–0.97)
GCS_{CT}	0.99 (0.97–1)	0.99 (0.99–1)
GLS_{CT}	0.96 (0.84–0.99)	0.97 (0.88–0.99)

Abbreviations: CI, confidence interval; GCS_{CT}, 4DCT-derived global circumferential strain; GLS_{CT}, 4DCT-derived global longitudinal strain; ICC, intraclass correlation coefficient; ϵ_{ll}^{CT}, 4DCT-derived regional longitudinal strain; ϵ_{cc}^{CT}, 4DCT-derived regional circumferential strain.

additional X-ray dose. In this study, the average dose was 2.8 mSv. The time frames away from the diastolic full mA views were at 20% of the full mA; from this, we can infer that approximately 50% of the total dose comes from the narrow diastolic R–R region used to obtain the CCTA, and 50% of the dose is used to map the temporal evolution of strain. If only end systolic strain was needed, the additional dose would be approximately 20% of an even lower total dose of 1.7mSv.

While the 4DCT- and CMR-derived strain estimates were strongly correlated, it is important to note that the two methods measure different strain quantities. The 4DCT method developed in this work estimates LV strains precisely *on* the endocardial surface, while the commercial CMR feature tracking method estimates the average strain averaged over each *myocardial* segment; therefore, the comparison made was between *endocardial* and "*mid-wall*" strains, respectively (Sec. 4.2 provides further information describing the quantitative relationship between endocardial and mid-wall strains). Additionally, the underlying methods of strain computation between the 4DCT and CMR methods were different. The 4DCT method extracts high-resolution point clouds delineating the textured endocardial surface for each pose of the LV and registers these point clouds across time using a nonrigid registration algorithm to derive 3D deformation fields across the cardiac cycle. The CMR feature tracking method interpolates the smooth endo- and epicardial contours detected in the 2D short- and long-axis CMR images at end diastole to

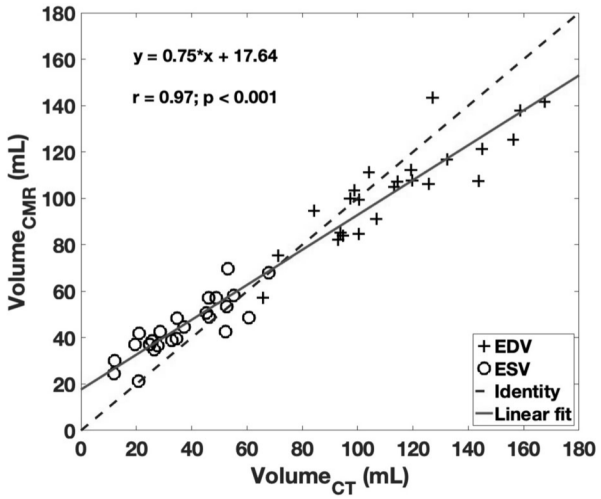


FIGURE 8 Relationship between 4DCT- and CMR-derived EDV and ESV estimates for all 24 subjects. EDV estimates are shown by the "+" symbol, while ESV are shown by "o."
Abbreviations : EDV, end diastolic volume; ESV, end systolic volume; Volume$_{CT}$, 4DCT-derived volume; Volume$_{CMR}$, CMR-derived volume.

form a deformable 3D model of the LV myocardium. A set of nodes are then mathematically placed at the mid-wall halfway between the detected endo- and epicardial boundaries, and an incompressible deformation model is fit to derive 3D displacement fields. The CMR strain estimation algorithm has been previously described in detail.[29,31,32]

4.1 | 4DCT-derived regional LV endocardial strain estimation

The developed method uses patches of radius 7.5 mm to sample the endocardial surface for strain estimation; the patches are densely sampled across the entire LV surface yielding high-resolution estimates of regional endocardial strains. The spatial resolution limit of the point-set registration technique utilized in this current work was previously investigated in the context of detecting regional wall motion abnormalities (WMA)[13] with RS$_{CT}$. It was reported that the size threshold for detection of WMA was between 14 mm and 19 mm in diameter; therefore, we expect the spatial resolution of the proposed strain estimation method to be similar.

We previously developed RS$_{CT}$, which is a 4DCT-derived metric that estimates regional endocardial shortening.[12,22] RS$_{CT}$ has been shown to be highly reproducible,[24] and has been validated using phantom experiments[13] and against CMR tagging in canine hearts.[23] RS$_{CT}$ is very robust as it estimates endocardial shortening independent of the cardiac coordinate system. The method developed in this study compliments RS$_{CT}$ in providing directional estimates of regional and global endocardial strains. Directional cardiac strains have been shown to have prognostic value in patients with specific cardiac diseases,[33–36] thus developing a comprehensive analysis pipeline for the estimation of regional directional endocardial strains from 4DCT was an unmet clinical need.

Additionally, the method is fully automated, except for the definition of the mitral valve and the LV outflow tract planes. The reproducibility of the segmentation procedure has been shown to be very high, both in this study and in a previous study.[24] With the rapid advancements made in the field of deep learning cardiac segmentation, we expect the method to be fully automated very soon.[37] In particular, we have been successful at automating the position of the mitral valve plane.[38] The high reproducibility of both LV strains and volumes helps solve a long-standing shortcoming of nonreproducible quantitative function measurements from echocardiography.[39–41]

We anticipate the performance of the developed 4DCT strain estimation method to improve with higher resolution, motion-corrected data[14] subjected to new deep learning networks for segmentation or direct strain estimation. Examination of the dependence of accuracy on dose will also permit the establishment of the minimum required dose for robust strain estimates. The developed method was applied to routinely acquired low-dose clinical CTA images, highlighting the applicability of the proposed method using these relatively "noisy" images. Additionally, the 24 subjects used in this study had relatively high BMIs, which also reduced image quality. Future studies will investigate the threshold for dose reduction that will permit the accurate and reproducible estimation of regional endocardial strains.

4.2 | Relationship between mid-wall and endocardial LV strains

Significant effort has been focused on developing CMR feature tracking as a method to estimate global and regional myocardial function.[42] In particular, the commercial feature tracking software used in this study (cvi42) has been shown to yield highly reproducible estimates of 3D LV strain[29] and has been used extensively to quantify myocardial strain.[30,43] The relationship between the 4DCT- and CMR-derived regional strains shown in Figure 6 confirmed that the proposed 4DCT method yields strains that are larger in magnitude. This relationship was expected because the 4DCT method estimates *endocardial* strain, whereas the CMR feature tracking method estimates the average myocardial strain within each AHA segment (similar to "mid-wall" strain). Equation (3) describes the simple relationship between mid-wall and endocardial circumferential strains for a pair of concentric circles, when the endocardial circle moves inward and the epicardial circle

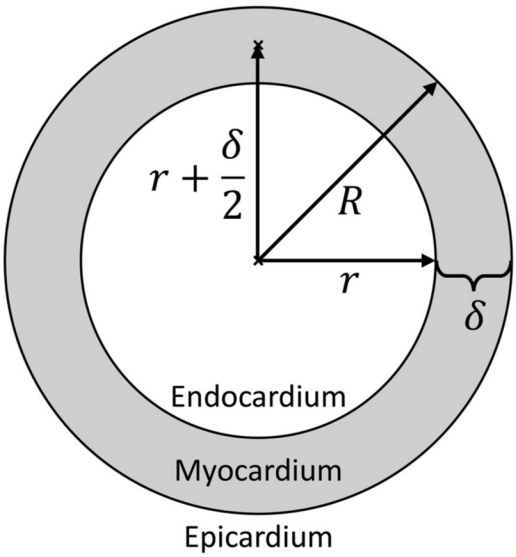


FIGURE 9 Graphical representation of a mid-cavity LV short axis slice. The grey region represents the myocardium, and the inner and outer circles represent the endocardium and the epicardium, respectively. r is the endocardial radius (LV internal radius), R is the epicardial radius, and $\delta = R - r$ is the myocardial wall thickness

remains fixed during systole:

$$\epsilon_{cc_{mid}} = \epsilon_{cc_{endo}} * \left(\frac{r}{r+R}\right), \quad (3)$$

where $\epsilon_{cc_{mid}}$ is the mid-wall circumferential strain, $\epsilon_{cc_{endo}}$ is the endocardial circumferential strain, and r and R are the endocardial and epicardial radii at end diastole, respectively as shown in Figure 9. Equation (3) corresponds to the $y = m \times x + c$ linear model used to fit the data between the 4DCT- and CMR-derived regional strains in Figure 6, where $m \equiv \frac{r}{r+R}$, $y \equiv \epsilon_{cc_{mid}}$, and $x \equiv \epsilon_{cc_{endo}}$. For the 24 cases used in this study, the average mid-cavity LV internal diameter was 46 mm, and the average wall thickness was 7 mm; therefore, using this very simple model $\frac{r}{r+R} = 0.43$, which is consistent with the measured value of 0.56 in Figure 6a. The theoretical model described above is not intended to be an accurate model to predict mid-wall from endocardial circumferential strains in human LVs (e.g., the assumption that the epicardium remains fixed is obviously too simple) but provides a simple understanding of their approximate relationship. The $\frac{r}{r+R}$ parameter is dependent on the endocardial and epicardial radii, which differ not only between subjects but also between the apex and base; however, the simple model shows that the mid-wall strain will be significantly lower in magnitude from the strain on the endocardium. Additionally, the slopes of the linear fits in Figure 7a,c also support our result of the 4DCT- and CMR-derived regional strains not being related by a slope of 1; while GCS_{CT} was related to EF_{CT} with a slope of −0.59, GCS_{MR} was related to EF_{MR} with a significantly lower slope of -0.25, highlighting that the mid-wall and endocardial strains scale differently with global LV function. It is also clear from Figure 7 that 4DCT provides much higher EF values than CMR; this offset is due to "counting blood pool voxels" in 4DCT images to measure LV chamber volume instead of calculating the volume contained within smooth endocardial contours on CMR; the endocardial contours from CMR are notoriously hard to reproduce.[44] The high reproducibility of the 4DCT blood pool volumes is a significant strength of the 4DCT method for evaluating cardiac function.

4.3 | Comparison with other 4DCT strain estimation methods

Previous studies have used 4DCT to estimate regional LV strain[17–21]; however, these studies are based on smooth contours that represent the endocardium and the epicardium. The new method proposed in this work takes advantage of the region within the CT image volume with the greatest contrast and quantity of fiducial markers: the boundary between the endocardium and the contrast-enhanced blood pool. Extraction of the spatially detailed blood pool boundary (vs. smooth contours) from 4DCT images and the estimation of local endocardial deformation from points on that endocardial boundary have been shown to be highly reproducible.[22,24,45] Manual guidance for the segmentation of epicardial and endocardial contours has long been a source of error and variability[44]; simple thresholding of the LV blood pool using a reproducible threshold (like Otsu's method[46]) to define the endocardial surface alleviates this problem.

4.4 | Significance of LV endocardial strain estimation

Previous studies have shown that endocardial function is more significantly affected than mid-wall or whole AHA segment myocardial function in acute ischemia[47] and nontransmural infarction,[48] highlighting the potential benefit of the accurate and reproducible estimation of regional endocardial function. The method developed in this study yields strains that are on the absolute endocardial boundary; thus, there is a very strong correlation between GCS and LVEF as shown in Figure 7a. The GCS strain estimates are closely tied to the global function of the LV as indicated by LVEF. Endocardial strain estimation also provides us with a larger dynamic range over which we can measure more subtle differences in regional LV function between pre- and post-therapy (e.g., TMVI[24]).

4.5 | Advantages of 4DCT

While other modalities such as CMR and echocardiography do not use ionizing radiation, the superior resolution and reproducibility of low-dose 4DCT offer significant advantages over other modalities in the estimation of regional cardiac function, especially with the recent developments in low-dose imaging. Modern 4DCT systems now yield images of full heart function acquired within a single heartbeat; this is especially useful when imaging patients with arrhythmias. Motion correction technologies have also significantly improved the temporal resolution of 4DCT, enabling the accurate and precise estimation of the timing of LV mechanics.[49] Additionally, significant effort has been focused on reducing the radiation dose from cardiac CT images. From dose surveys obtained in 2007 and 2017, it was reported that the dose received from CT angiography images was reduced by 78%.[50] Clinical cardiac CT images are now acquired with radiation doses between [0.5 4] mSv,[7,8] which is comparable to the annual radiation dose received from natural sources.[51] Additionally, we can expect the dose to be lowered further with the advent of photon-counting detectors, more powerful X-ray generators at low kVp, and the use of deep learning.[52]

4.6 | Limitations

This study uses 24 subjects with both 4DCT and CMR scans acquired just a few hours apart which is a rare dataset, facilitating a direct comparison of strain estimates between two methods in the same subjects. While the 4DCT- and CMR-derived regional strains correlated well, future studies should investigate the relationship between the two methods in a larger cohort of subjects.

Despite this dataset having many favorable characteristics, any comparisons between imaging modalities have obvious limitations: (1) the 4DCT-derived strain values were estimated on the endocardial surface, while the CMR-derived strain values were measured as the average strain within the relatively large individual AHA myocardial segments, (2) the 4DCT images were acquired upon inspiration within one heartbeat whereas the CMR images were acquired during 12 independent breath-holds, at end expiration by acquiring data over 8–10 heartbeats, (3) while the CMR scans were always acquired first, the ∼4 h delay between CMR and CT could have led to differences in cardiovascular loading conditions, and lastly (4) the 4DCT scans were acquired usually after the administration of metoprolol and nitroglycerin to optimize CCTA image quality. Due to these unavoidable factors, perfect agreement between the two modalities is not expected; however, most comparative studies are subject to even longer delays between exams.

The proposed 4DCT based strain method does not require contouring the endocardium and epicardium; thus, we found highly reproducible estimates of regional endocardial strains. While the lack of epicardial contours prevents the estimation of radial strain, new deep learning techniques for achieving consistent segmentation of the epicardium will soon make this possible. Additionally, as is the case with all techniques that depend on an estimate of the location of the endocardial wall, our 4DCT strain map has "blind spots" at the papillary muscle insertion and requires interpolation from the surrounding nonpapillary muscle tissue.

5 | CONCLUSIONS

A method to obtain high resolution estimates of regional LV endocardial circumferential and longitudinal strains from 4DCT images was developed. The method was applied on low-dose clinical 4DCT images acquired within a single heartbeat. The method was highly reproducible and yielded regional endocardial strain estimates that correlated well with segmental strain estimates obtained from CMR feature tracking. The encouraging results reported in this study highlight the potential utility of 4DCT in regional cardiac function assessment for the diagnosis and management of cardiac diseases.

ACKNOWLEDGMENTS

The authors thank Justin Roberts and Jerry Loichinger of Circle Cardiovascular Imaging Inc. for all their valuable support and assistance with cvi42. This work was supported by grants from the National Institutes of Health, USA (NIH F31HL151183, T32HL105373, R01HL144678, and 1ZIAHL006220) and the American Heart Association (AHA 20PRE35210261). This work was partially funded by projects RTI2018-098682-B-I00 (MCIU/AEI/FEDER,UE) by the Spanish ministry of Science and Innovation, co-funded by the European Union ERDF (European Regional Development Fund).

CONFLICT OF INTEREST

McVeigh holds founder shares in Clearpoint Neuro Inc. and receives research funding from GE Healthcare, Abbott Medical, and Pacesetter Inc.

REFERENCES

1. Cho G-Y, Marwick TH, Kim H-S, Kim M-K, Hong K-S, Oh D-J. Global 2-Dimensional strain as a new prognosticator in patients with heart failure. *J Am Coll Cardiol*. 2009;54(7):618-624. https://doi.org/10.1016/j.jacc.2009.04.061
2. Edvardsen T, Skulstad H, Aakhus S, Urheim S, Ihlen H. Regional myocardial systolic function during acute myocardial ischemia assessed by strain Doppler echocardiography. *J Am Coll Cardiol*. 2001;37(3):726-730. https://doi.org/10.1016/S0735-1097(00)01160-8

3. Leclercq C, Faris O, Tunin R, et al. Systolic improvement and mechanical resynchronization does not require electrical synchrony in the dilated failing heart with left bundle-branch block. *Circulation*. 2002;106(14):1760-1763. https://doi.org/10.1161/01.CIR.0000035037.11968.5C
4. Mignot A, Donal E, Zaroui A, et al. Global longitudinal strain as a major predictor of cardiac events in patients with depressed left ventricular function: a multicenter study. *J Am Soc Echocardiogr*. 2010;23(10):1019-1024. https://doi.org/10.1016/j.echo.2010.07.019
5. Potter E, Marwick TH. Assessment of left ventricular function by echocardiography. *JACC Cardiovasc Imaging*. 2018;11(2):260-274. https://doi.org/10.1016/j.jcmg.2017.11.017
6. Haji K, Marwick TH. Clinical utility of echocardiographic strain and strain rate measurements. *Curr Cardiol Rep*. 2021;23(3):18. https://doi.org/10.1007/s11886-021-01444-z
7. Chen MY, Shanbhag SM, Arai AE. Submillisievert median radiation dose for coronary angiography with a second-generation 320—detector row CT scanner in 107 consecutive patients. *Radiology*. 2013;267(1):76-85. https://doi.org/10.1148/radiol.13122621
8. Contijoch FJ, Groves DW, Chen Z, Chen MY, McVeigh ER. A novel method for evaluating regional RV function in the adult congenital heart with low-dose CT and SQUEEZ processing. *Int J Cardiol*. 2017;249:461-466. https://doi.org/10.1016/j.ijcard.2017.08.040
9. Kwan AC, Pourmorteza A, Stutman D, Bluemke DA, Lima JAC. Next-generation hardware advances in CT: cardiac applications. *Radiology*. 2021;298(1):3-17. https://doi.org/10.1148/radiol.2020192791
10. Cruz-Bastida JP, Gomez-Cardona D, Li K, et al. Hi-Res scan mode in clinical MDCT systems: experimental assessment of spatial resolution performance. *Med Phys*. 2016;43(5):2399-2409. https://doi.org/10.1118/1.4946816
11. Manohar A, Rossini L, Colvert G, et al. Regional dynamics of fractal dimension of the left ventricular endocardium from cine computed tomography images. *J Med Imaging*. 2019;6(04):1. https://doi.org/10.1117/1.JMI.6.4.046002
12. Pourmorteza A, Schuleri KH, Herzka DA, Lardo AC, McVeigh ER. A new method for cardiac computed tomography regional function assessment. *Circ Cardiovasc Imaging*. 2012;5(2):243-250. https://doi.org/10.1161/CIRCIMAGING.111.970061
13. Manohar A, Colvert GM, Schluchter A, Contijoch F, McVeigh ER. Anthropomorphic left ventricular mesh phantom: a framework to investigate the accuracy of SQUEEZ using coherent point drift for the detection of regional wall motion abnormalities. *J Med Imaging*. 2019;6(04):1. https://doi.org/10.1117/1.JMI.6.4.045001
14. Pack JD, Manohar A, Ramani S, et al. Four-dimensional computed tomography of the left ventricle, Part I: motion artifact reduction. *Med Phys*. Published online 30 May 2022. https://doi.org/10.1002/mp.15709
15. Boyd AC, Schiller NB, Thomas L. Principles of transthoracic echocardiographic evaluation. *Nat Rev Cardiol*. 2015;12(7):426-440. https://doi.org/10.1038/nrcardio.2015.57
16. Maron DJ, Hochman JS, Reynolds HR, et al. Initial invasive or conservative strategy for stable coronary disease. *N Engl J Med*. 2020;382(15):1395-1407. https://doi.org/10.1056/nejmoa1915922
17. Lamash Y, Fischer A, Carasso S, Lessick J. Strain analysis from 4-D cardiac CT image data. *IEEE Trans Biomed Eng*. 2015;62(2):511-521. https://doi.org/10.1109/TBME.2014.2359244
18. Gupta V, Lantz J, Henriksson L, et al. Automated three-dimensional tracking of the left ventricular myocardium in time-resolved and dose-modulated cardiac CT images using deformable image registration. *J Cardiovasc Comput Tomogr*. 2018;12(2):139-148. https://doi.org/10.1016/j.jcct.2018.01.005
19. Gegenava T, van der Bijl P, Hirasawa K, et al. Feature tracking computed tomography-derived left ventricular global longitudinal strain in patients with aortic stenosis: a comparative analysis with echocardiographic measurements. *J Cardiovasc Comput Tomogr*. 2020;14(3):240-245. https://doi.org/10.1016/j.jcct.2019.11.004
20. Peled Z, Lamash Y, Carasso S, et al. Automated 4-dimensional regional myocardial strain evaluation using cardiac computed tomography. *Int J Cardiovasc Imaging*. 2020;36(1):149-159. https://doi.org/10.1007/s10554-019-01696-5
21. Vach M, Vogelhuber J, Weber M, et al. Feasibility of CT-derived myocardial strain measurement in patients with advanced cardiac valve disease. *Sci Rep*. 2021;11(1):8793. https://doi.org/10.1038/s41598-021-88294-5
22. McVeigh ER, Pourmorteza A, Guttman M, et al. Regional myocardial strain measurements from 4DCT in patients with normal LV function. *J Cardiovasc Comput Tomogr*. 2018;12(5):372-378. https://doi.org/10.1016/j.jcct.2018.05.002
23. Pourmorteza A, Chen MY, van der Pals J, Arai AE, McVeigh ER. Correlation of CT-based regional cardiac function (SQUEEZ) with myocardial strain calculated from tagged MRI: an experimental study. *Int J Cardiovasc Imaging*. 2016;32(5):817-823. https://doi.org/10.1007/s10554-015-0831-7
24. Colvert GM, Manohar A, Contijoch FJ, et al. Novel 4DCT method to measure regional left ventricular endocardial shortening before and after transcatheter mitral valve implantation. *Struct Hear*. 2021;5(4):410-419. https://doi.org/10.1080/24748706.2021.1934617
25. Shehata ML, Cheng S, Osman NF, Bluemke DA, Lima JA. Myocardial tissue tagging with cardiovascular magnetic resonance. *J Cardiovasc Magn Reson*. 2009;11(1):55. https://doi.org/10.1186/1532-429X-11-55
26. Yushkevich PA, Piven J, Hazlett HC, et al. User-guided 3D active contour segmentation of anatomical structures: significantly improved efficiency and reliability. *Neuroimage*. 2006;31(3):1116-1128. https://doi.org/10.1016/j.neuroimage.2006.01.015
27. Myronenko A, Xubo Song. Point set registration: coherent point drift. *IEEE Trans Pattern Anal Mach Intell*. 2010;32(12):2262-2275. https://doi.org/10.1109/TPAMI.2010.46
28. Cerqueira MD, Weissman NJ, Dilsizian V, et al. Standardized myocardial segmentation and nomenclature for tomographic imaging of the heart. *Circulation*. 2002;105(4):539-542. https://doi.org/10.1161/hc0402.102975
29. Liu B, Dardeer AM, Moody WE, et al. Reference ranges for three-dimensional feature tracking cardiac magnetic resonance: comparison with two-dimensional methodology and relevance of age and gender. *Int J Cardiovasc Imaging*. 2017;34(5):761-775. https://doi.org/10.1007/s10554-017-1277-x
30. Qu Y-Y, Paul J, Li H, Ma G-S, Buckert D, Rasche V. Left ventricular myocardial strain quantification with two- and three-dimensional cardiovascular magnetic resonance based tissue tracking. *Quant Imaging Med Surg*. 2021;11(4):1421-1436. doi:10.21037/qims-20-635
31. Bistoquet A, Oshinski J, Skrinjar O. Left ventricular deformation recovery from cine MRI using an incompressible model. *IEEE Trans Med Imaging*. 2007;26(9):1136-1153. https://doi.org/10.1109/TMI.2007.903693
32. Bistoquet A, Oshinski J, Skrinjar O. Myocardial deformation recovery from cine MRI using a nearly incompressible biventricular model. *Med Image Anal*. 2008;12(1):69-85. https://doi.org/10.1016/j.media.2007.10.009
33. Mangion K, Carrick D, Carberry J, et al. Circumferential strain predicts major adverse cardiovascular events following an acute ST-segment–elevation myocardial infarction. *Radiology*. 2019;290(2):329-337. https://doi.org/10.1148/radiol.2018181253
34. Namazi F, van der Bijl P, Hirasawa K, et al. Prognostic value of left ventricular global longitudinal strain in patients with secondary mitral regurgitation. *J Am Coll Cardiol*. 2020;75(7):750-758. https://doi.org/10.1016/j.jacc.2019.12.024

35. Oikonomou EK, Kokkinidis DG, Kampaktsis PN, et al. Assessment of prognostic value of left ventricular global longitudinal strain for early prediction of chemotherapy-induced cardiotoxicity. *JAMA Cardiol*. 2019;4(10):1007. https://doi.org/10.1001/jamacardio.2019.2952
36. Gao X, Abdi M, Auger DA, et al. Cardiac magnetic resonance assessment of response to cardiac resynchronization therapy and programming strategies. *JACC Cardiovasc Imaging*. Published online 6th December 2021. https://doi.org/10.1016/j.jcmg.2021.06.015
37. Chen C, Qin C, Qiu H, et al. Deep Learning for Cardiac Image Segmentation: A Review. *Front Cardiovasc Med*. 2020;7(March). https://doi.org/10.3389/fcvm.2020.00025
38. Vigneault DM, Contijoch F, Bridge CP, Lowe K, Jan C, McVeigh ER. M-SiSSR: regional endocardial function using multilabel simultaneous subdivision surface registration. In: *Functional Imaging and Modeling of the Heart*. Springer, Cham; 2021:242-252. https://doi.org/10.1007/978-3-030-78710-3_24
39. Mirea O, Pagourelias ED, Duchenne J, et al. Variability and reproducibility of segmental longitudinal strain measurement. *JACC Cardiovasc Imaging*. 2018;11(1):15-24. https://doi.org/10.1016/j.jcmg.2017.01.027
40. Mirea O, Pagourelias ED, Duchenne J, et al. Intervendor differences in the accuracy of detecting regional functional abnormalities. *JACC Cardiovasc Imaging*. 2018;11(1):25-34. https://doi.org/10.1016/j.jcmg.2017.02.014
41. Badano LP, Muraru D. The good, the bad, and the ugly of using left ventricular longitudinal myocardial deformation by speckle-tracking echocardiography to assess patients after an acute myocardial infarction. *Circ Cardiovasc Imaging*. 2017;10(7):1-3. https://doi.org/10.1161/CIRCIMAGING.117.006693
42. Rahman ZU, Sethi P, Murtaza G, et al. Feature tracking cardiac magnetic resonance imaging: a review of a novel non-invasive cardiac imaging technique. *World J Cardiol*. 2017;9(4):312. https://doi.org/10.4330/wjc.v9.i4.312
43. Zhang Y, Mui D, Chirinos JA, et al. Comparing cardiovascular magnetic resonance strain software packages by their abilities to discriminate outcomes in patients with heart failure with preserved ejection fraction. *J Cardiovasc Magn Reson*. 2021;23(1):55. https://doi.org/10.1186/s12968-021-00747-y
44. Karamitsos T, Hudsmith L, Selvanayagam J, Neubauer S, Francis J. Operator induced variability in left ventricular measurements with cardiovascular magnetic resonance is improved after training. *J Cardiovasc Magn Reson*. 2007;9(5):777-783. https://doi.org/10.1080/10976640701545073
45. Pourmorteza A, Keller N, Chen R, et al. Precision of regional wall motion estimates from ultra-low-dose cardiac CT using SQUEEZ. *Int J Cardiovasc Imaging*. 2018;34(8):1277-1286. https://doi.org/10.1007/s10554-018-1332-2
46. Otsu N. A threshold selection method from gray-level histograms. *IEEE Trans Syst Man Cybern*. 1979;9(1):62-66. https://doi.org/10.1109/TSMC.1979.4310076
47. Howard-Quijano K, McCabe M, Cheng A, et al. Left ventricular endocardial and epicardial strain changes with apical myocardial ischemia in an open-chest porcine model. *Physiol Rep*. 2016;4(24):e13042. doi:10.14814/phy2.13042
48. Becker M, Ocklenburg C, Altiok E, et al. Impact of infarct transmurality on layer-specific impairment of myocardial function: a myocardial deformation imaging study. *Eur Heart J*. 2009;30(12):1467-1476. https://doi.org/10.1093/eurheartj/ehp112
49. Manohar A, Pack JD, Schluchter AJ, McVeigh ER. Four-dimensional computed tomography of the left ventricle, Part II: estimation of mechanical activation times. *Med Phys*. Published online March 2, 2022. https://doi.org/10.1002/mp.15550
50. Stocker TJ, Deseive S, Leipsic J, et al. Reduction in radiation exposure in cardiovascular computed tomography imaging: results from the PROspective multicenter registry on radiaTion dose Estimates of cardiac CT angIOgraphy iN daily practice in 2017 (PROTECTION VI). *Eur Heart J*. 2018;39(41):3715-3723. https://doi.org/10.1093/eurheartj/ehy546
51. Bolus NE. NCRP report 160 and what it means for medical imaging and nuclear medicine. *J Nucl Med Technol*. 2013;41(4):255-260. https://doi.org/10.2967/jnmt.113.128728
52. Lell MM, Kachelrieß M. Recent and upcoming technological developments in computed tomography. *Invest Radiol*. 2020;55(1):8-19. https://doi.org/10.1097/RLI.0000000000000601

How to cite this article: Manohar A, Colvert GM, Ortuño JE, et al. Regional left ventricular endocardial strains estimated from low-dose 4DCT: Comparison with cardiac magnetic resonance feature tracking. *Med Phys*. 2022;49:5841–5854. https://doi.org/10.1002/mp.15818